How to Cite: Burkitbayeva, B.D., Adeloye, A.O., Miftakhova, A.F., Jumanova, R.Zh., Beisenova, G.S., Argimbayeva, A.M., Seit, G., Bakhytzhan, Ye.G., & Smail, A.B. (2026). Comparative Electrochemical and Corrosion Inhibition Assessment of Commercial Tannic Acid, Crude Extracts, and *n*-Butanol Fractions of *Quercus robur Stem Bark*. *Eurasian Journal of Chemistry, 31, 3(123), 129–143.* https://doi.org/10.31489/2959-0663/3-26-13

CHEMICAL TECHNOLOGY

Article

Received: 25 June 2026 | Revised: 1 September 2026 |
Accepted: 8 September 2026 | Published online: 10 September 2026

UDC 66.097.8:620.197.3:544.654 https://doi.org/10.31489/2959-0663/3-26-13

Bibisara D. Burkitbayeva[1], Adewale O. Adeloye[1], Alfira F. Miftakhova[1], Raigul Zh. Jumanova[1], Gulmira S. Beisenova[1]*, Akmaral M. Argimbayeva[1], Gulzhan Seit[1], Yeldana G. Bakhytzhan[1], Aruzhan B. Smail[1]

al-Farabi Kazakh National University, Almaty, Kazakhstan
*(*Corresponding author's e-mail: beisenova.gumi@gmail.com)*

Comparative Electrochemical and Corrosion Inhibition Assessment of Commercial Tannic Acid, Crude Extracts, and *n*-Butanol Fractions of Quercus robur Stem Bark

In this study, crude aqueous-ethanolic extract and n-butanol fraction of Quercus robur stem bark were obtained, and their corrosion-inhibition performance on mild steel in 1 M HCl was evaluated while their performances are compared to the commercial tannic acid used as standard. Corrosion inhibition was assessed by potentiodynamic polarization at 200 mg L^{-1} after 1 hour of immersion. The n-butanol fraction exceeded the 71.9 % efficiency of the crude extract, though remaining below the 98.2 % maximum efficiency observed for the tannic acid standard at 1000 mg L^{-1}. Polarization curve shifts support classifying the tannin-containing samples as mixed-type inhibitors. Adsorption-isotherm analysis showed model-dependent behavior: the Freundlich model provided the highest R^2 for the crude extract, while the Langmuir model provided the highest R^2 for the n-butanol fraction and tannic acid. These fits represent empirical descriptions of concentration-dependent inhibition rather than direct molecular mechanisms. For commercial tannic acid, the standard Gibbs free energy of adsorption ΔG^0_{ads} as approximately -33.3 kJ mol^{-1}, indicating thermodynamically favorable adsorption. Overall, solvent fractionation improved inhibition performance. These findings indicate the n-butanol fraction's potential as a plant-derived inhibitor. Further phytochemical investigation, isolation and characterization are required to properly identify the active constituents underlying the adsorption mechanisms.

Keywords: *Quercus robur*, *n*-butanol fraction, commercial tannic acid, corrosion inhibitor, mild steel, potentiodynamic polarization, adsorption isotherms.

1 Introduction

Corrosion of metals and alloys remains a critical, resource-intensive challenge across industrial sectors such as oil and gas production, pipeline infrastructure, construction, and water supply systems. Beyond causing severe economic losses through structural degradation, corrosion indirectly accelerates global greenhouse gas emissions. While conventional corrosion mitigation relies heavily on inorganic inhibitors (such as chromates, phosphates, and silicates) and synthetic organic compounds, their toxicity and severe environmental risks have necessitated a transition toward sustainable alternatives [1, 2]. Consequently, recent research has increasingly focused on biodegradable, plant-derived green inhibitors.

Among naturally occurring plant-derived compounds, tannins extracted from bark, seeds, and leaves have attracted substantial attention due to their structural features and potential corrosion-inhibiting properties. Tannins are polyphenolic compounds generally classified into hydrolysable tannins, which include gallic acid-derived structures, and condensed tannins, consisting mainly of oligomeric and polymeric proanthocyanidins. *Quercus robur* bark has been reported as a source of tannin-containing polyphenolic compounds, including hydrolysable and condensed tannin-related constituents [3-5]. Owing to the presence

© 2026 The Authors. This is an open access article under the CC BY-NC-ND license (http://creativecommons.org/licenses/by-nc-nd/4.0/)

of multiple phenolic hydroxyl groups and aromatic structures, tannin-containing plant materials have attracted increasing interest as potential environmentally compatible corrosion inhibitors. While historically utilized in medicine and leather processing, these polyphenolic materials are increasingly being investigated for applications in materials science, including corrosion protection.

The corrosion-inhibition activity of plant tannins has commonly been attributed to their abundant hydroxyl groups and aromatic rings, which may act as electron-donating sites [6]. Previous studies have proposed that tannin-containing compounds can adsorb on metal surfaces and interact with iron species, potentially forming iron–tannate complexes that contribute to the formation of a protective interfacial layer [7, 8]. Such interactions have been proposed to contribute to corrosion inhibition in aggressive hydrochloric acid environments, which are widely encountered in industrial pickling, acid cleaning, and scale removal. Electrochemical studies have also reported tannin-containing inhibitors as mixed-type inhibitors, based on their effects on both the anodic and cathodic branches of polarization curves [8, 9].

Plant-derived tannins have demonstrated corrosion-inhibition activity under diverse experimental conditions. For instance, Gelam tree bark tannins achieved 89.66 % inhibition efficiency for mild steel in 1 M HCl [10], quebracho tannin extract showed corrosion-inhibition effects in 3.5 % NaCl solution [11], and commercial tannins (TG 3300) reached approximately 85 % inhibition efficiency at pH 10.5 [12]. Previous studies have associated these protective effects with adsorption of tannin-containing species and possible interactions between phenolic constituents and iron species, including the formation of iron–tannate complexes.

In the present study, a crude aqueous-ethanolic extract of *Quercus robur* stem bark was subjected to sequential solvent fractionation, and the resulting *n*-butanol fraction was evaluated for corrosion inhibition of mild steel in 1 M HCl. The crude extract and the *n*-butanol fraction were characterized using FT-IR spectroscopy, and UV-Vis spectrophotometry, while commercial tannic acid was used as a reference material. Their corrosion-inhibition performance was comparatively evaluated by potentiodynamic polarization at different concentrations and immersion times. In addition, the concentration-dependent inhibition data were analyzed using Langmuir, Freundlich, and Temkin adsorption-isotherm models. The study therefore provides a comparative assessment of the crude extract, its *n*-butanol fraction, and commercial tannic acid, with particular emphasis on the effect of solvent fractionation on tannin-equivalent content and corrosion-inhibition performance.

2 Experimental

2.1 Preparation and Extraction of Quercus Robur Bark

Granulated commercial oak (Quercus robur) bark was obtained from Zerde-Fito LLP (Kazakhstan) and used as-supplied. A 1000 g portion of the dried bark was treated with a 1:1 (v/v) water-ethanol solvent mixture (3 L) as illustrated in Figure 1. Following extraction, the liquid suspension was filtered to completely remove residual solid plant biomass. The resulting dark-brown filtrate was subsequently concentrated under reduced pressure using an IKA RV 05 Basic rotary evaporator coupled with an HB4 Basic heating bath (IKA-Werke GmbH & Co. KG, Germany). To protect thermolabile phenolic compounds against thermal degradation, distillation was maintained strictly at a controlled temperature range not exceeding 40–45 ^{o}C [13]. This optimized recovery protocol yielded 83.27 g of a highly concentrated, dark-brown viscous ethanolic extract which was further subjected to solvent-solvent partitioning to obtain the n-butanol fraction used for subsequent characterization and corrosion-inhibition evaluation.

2.2 Liquid-Liquid Fractionation

A portion of the dried extract (50.0 g, dry weight basis) was re-dissolved in 1.0 L of distilled water and successively partitioned using solvents of increasing polarity following a standard phytochemical fractionation procedure [14]: n-hexane (500–600 mL), dichloromethane (1000 mL), ethyl acetate (1400 mL), and n-butanol (1400 mL). Concentration in vacuo yielded the n-hexane fraction (0.85 g), dichloromethane fraction (1.862 g), ethyl acetate fraction (7.705 g), n-butanol fraction (16.332 g), and residual aqueous fraction (20.140 g). This sequential solvent hierarchy — transitioning from non-polar to high-polarity media effectively fractionated the complex phytochemical matrix, with dominant mass recoveries concentrated in the polar n-butanol and aqueous phases, reflecting the inherent abundance of hydroxyl-rich polyphenolic constituents in Quercus robur. The cumulative recovery mass accounted for approximately 93.8 % of the initial extract load, with the minor mass differential (<6.2 %) well within expected technical parameters due to interfacial retention and mechanical transfer losses during multi-step liquid-liquid extraction.

2.3 Thin-Layer chromatography (TLC)

The TLC plates were developed using carefully optimized solvent systems was utilized strictly as a qualitative fingerprinting and comparative tool, rather than a quantitative metric to resolve the polar constituents within the n-butanol fraction. Following development, visualization was achieved via exposure to iodine vapors and subsequent inspection under ultraviolet light at wavelengths of 254 nm and 366 nm to detect UV-active and fluorescent phytochemical metabolites. Distinct, well-resolved spots with reproducible R_f values were successfully recorded, mapping the phytochemical distributions in the fraction as compared to the standard commercial tannic acid.

2.4 Fourier-Transform Infrared (FT-IR) Spectroscopy

FT-IR spectra of commercial tannic acid (ACS reagent, Sigma-Aldrich, Merck KGaA, Germany, catalog no. 403040-100G; manufactured in China), the crude ethanolic extract, and the n-butanol fraction were acquired using an ALPHA II FT-IR spectrometer equipped with an ATR module and the ATR-LIB-COMPLETE spectral library (Bruker, Germany).

2.5 UV-Vis. Absorption Spectrophotometry

The total tannin content in the crude plant material was determined in accordance with the standardized protocol outlined in the State Pharmacopoeia of the Republic of Kazakhstan, as described in a recent study [15]. Quantitative evaluation of the n-butanol fraction was performed using a Hanon i3 UV-Vis spectrophotometer (Jinan Hanon Instruments Co., Ltd., China). Measurements were conducted at the characteristic absorption maximum of tannins, with quantification established via the linear relationship between solution concentration and absorbance at 290 nm in accordance with the Beer-Lambert law (Equation 1).

2.6 Preparation of Standard and Reagent Solutions

Quantitative estimation of the total tannin content in the crude ethanolic extract and its derived n-butanol fraction was performed spectrophotometrically using tannic acid as the analytical standard. A primary stock standard solution (1.0 g L^{-1}) was prepared by dissolving 1.000 g of analytical-grade tannic acid in distilled water and diluting to a final volume of 1000 mL. To prevent oxidative degradation of the polyphenolic structures during the assay, a freshly prepared 0.2 % (w/v) sodium bisulfite solution was utilized throughout the procedure.

A reference blank solution was prepared by dissolving 0.042 g of benzoic acid in 100 mL of distilled water, from which a 2.0 mL aliquot was further diluted to 10.0 mL with distilled water. For calibration, precise working aliquots ranging from 6.0 mL to 6.8 mL of the stock tannic acid solution were transferred into volumetric flasks. Each mixture was treated with 50.0 mL of the 0.2 % sodium bisulfite protective solution, 2.5 mL of a 0.01 M $FeCl_3$ chromogenic reagent, and 50.0 mL of distilled water, followed by thorough homogenization and dilution to volume.

Absorbance measurements of the resulting ferric-tannate complexes were recorded at a wavelength of 290 nm using 1 cm quartz cuvettes against the prepared reference blank for baseline correction. Final concentrations and total tannin yields were quantified in strict accordance with the Beer-Lambert law.

$$A = \varepsilon cl \quad (1)$$

where A is the absorbance, ε is the molar absorptivity coefficient, c is the concentration, and l is the optical path length.

2.7 Electrochemical Measurements

The corrosion-inhibition performance of the investigated tannin-containing samples was evaluated using potentiodynamic polarization, which is based on the continuous variation of the electrode potential at a predetermined scan rate while recording the resulting current response. This method enables evaluation of corrosion-inhibition performance and assessment of changes in the anodic and cathodic polarization behavior of the steel.

Electrochemical measurements were performed using an Autolab PGSTAT302N potentiostat/galvanostat. All experiments were conducted in a conventional three-electrode electrochemical cell consisting of a mild steel working electrode with an exposed surface area of 0.1256 cm^2, a platinum counter electrode, and an Ag/AgCl reference electrode.

Potentiodynamic polarization measurements were carried out in the potential range from –0.30 to +0.30 V relative to the open-circuit potential (OCP) at a scan rate of 2 mV s^{-1}. For each inhibitor concentration and immersion condition, three independent electrochemical measurements were performed using three

separate mild-steel specimens (n = 3). Each specimen was freshly prepared and polished prior to an individual electrochemical measurement. The reported electrochemical parameters are presented as mean ± standard deviation (SD) of the three independent measurements.

All electrochemical measurements were performed at room temperature (approximately 25 °C). Prior to testing, steel specimens were sequentially polished with abrasive papers of different grit sizes, rinsed with distilled water and acetone, and finally dried in air. This procedure was used to remove surface contaminants and obtain comparable initial surface conditions for the electrochemical measurements.

To evaluate the inhibitory performance of the investigated extracts, steel specimens were immersed in 1 M HCl solutions containing inhibitor concentrations ranging from 200 to 1200 mg L^{-1}. Polarization measurements were performed either immediately after immersion or after 1 h of immersion.

For Tafel analysis, linear portions of the anodic and cathodic polarization branches approximately 50–100 mV from the corrosion potential (E_{corr}) were used for extrapolation.

The inhibition efficiency was evaluated from the polarization parameters and corrosion rates calculated from the electrochemical data according to the following equation 2 [10]:

$$\eta(\%) = \frac{j_{corr}^{0} - j_{corr}}{j_{corr}^{0}} \times 100\% \quad (2)$$

where j_{corr}^{0} s the corrosion current density in the uninhibited solution (A cm^{-2}), and j_{corr} is the corrosion current density in the presence of the tannin-containing inhibitor (A cm^{-2}).

3 Results and Discussion

3.1 Extraction, Solvent-Solvent Partitioning of Quercus robur Bark and TLC profiles

The systematic workflow for the extraction and sequential solvent-solvent partitioning of the Quercus robur bark ethanolic extract is detailed in Figure 1. Sequential solvent-solvent partitioning facilitated a polarity-directed fractionation of the crude extract. The negligible yield recorded for the n-hexane fraction reflects a sparse concentration of non-polar constituents, such as aliphatic lipids and waxes, within the Quercus robur bark matrix. Conversely, the prominent quantitative recoveries observed across the ethyl acetate, n-butanol, and the residual aqueous fractions underscore a strong predominance of polar metabolites. This macroscopic distribution pattern aligns directly with the chemical profile of polyhydroxylated phenolic compounds, whose numerous hydroxyl groups and extensive hydrogen-bonding capacity govern their preferential partitioning into polar media, such structural features further corroborated by prominent infrared (IR) spectroscopic signals, notably the broad O-H stretching and aromatic C=C skeletal vibrations [16].

While exhaustive isolation of individual pure phytochemical constituents fell outside the immediate scope of this investigation, we optimized mobile phase systems established via preliminary TLC screening successfully mapped the complex phytochemical distribution of the crude matrix where solvent systems for column chromatography were developed. Typical thin-layer chromatography (TLC) profiles of crude ethanolic extract (A1), ethyl acetate fraction (A2), n-butanol fraction (A3) and commercial tannic acid (A4) are shown (Figure 2).

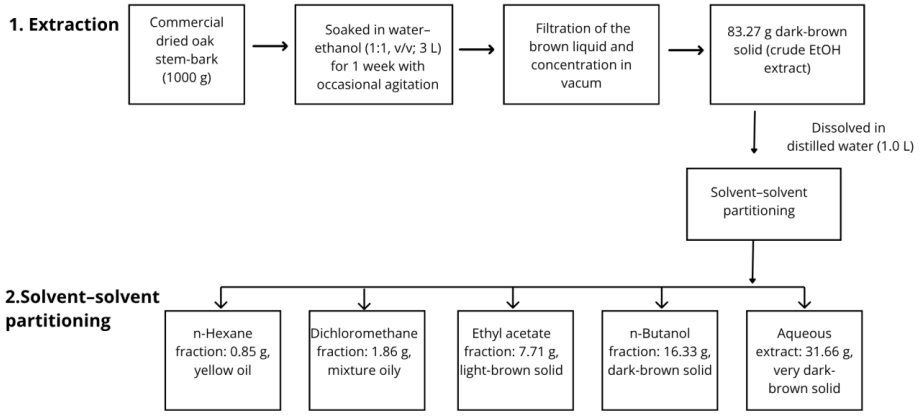

Figure 1. Extraction and Fractionation Scheme of *Quercus robur* Bark

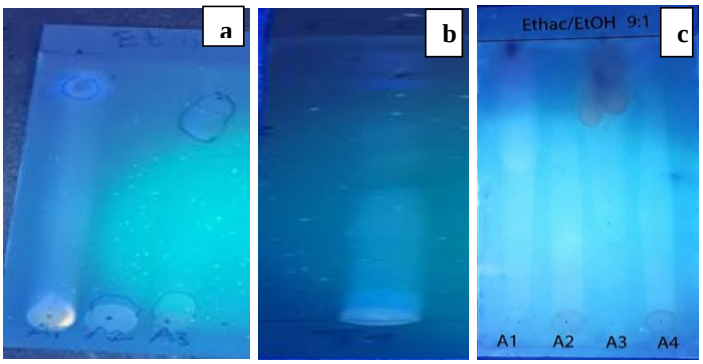

Figure 2. A typical TLC plates used for solvent system development and phytochemical constituents evaluation: Plate (a): crude ethanolic extract (**A1**), ethyl acetate (**A2**), *n*-butanol fraction (**A3**); Plate (b): commercial tannic acid, (TA)); and Plate (c): (**A1**) crude extract, (**A2**) ethyl acetate fraction, (**A3**) *n*-butanol fraction, and (**A4**) commercial tannic acid in ethyl acetate (100 %, volume, plates (a) and (b)); or ethyl acetate-ethanol (9:1, v/v). as mobile phase (plate c).

3.2 Comparative Analysis of FTIR Spectroscopic Studies of Commercial Tannic Acid, Crude Extract and n-Butanol fraction

The FT-IR spectral of the crude ethanolic extract and n-butanol fraction recorded within the 4000-400 cm^{-1} region, exhibits characteristic vibrational frequencies that are comparable to the functional groups observed in the FT-IR spectrum of the commercial tannic acid used as standard. For the commercial tannic acid — chemical structure as shown in Figure 3, and previously reported to be a complex and varying mixture of different gallotannins and simpler galloylglucoses [17]. The broad absorption band observed at 3191.22 cm^{-1} is attributed to the stretching vibration of hydroxyl υ(O–H) groups, indicative of an extensive hydrogen-bonding network within the molecular framework. A very weak band detected at 2890.66 cm^{-1} corresponds to the asymmetric and symmetric stretching vibrations of methylene (CH_2) groups.

The prominent sharp peaks resolved at 1701.96 cm^{-1} and 1697.34 cm^{-1} are assigned to carbonyl υ(C=O) stretching modes associated with the galloyl and ester functionalities. The distinct peak at 1604.66 cm^{-1} peak is characteristic of the skeletal aromatic ring stretching vibration υ(C=C). Furthermore, the absorption band at 1442.83 cm^{-1} is assigned to aromatic methine in-plane bending or skeletal vibrations υ(C–H), while the peak at 1306.98 cm^{-1} corresponds to the symmetric stretching mode of carboxylate υ(–COO–) species. Finally, the intense absorption bands observed at 1174.86 cm^{-1} and 1010.23 cm^{-1} are ascribed to the υ(C–O–C) stretching vibrations of the ester and ether linkages inherent to the pyrogallol and glucose core structures [18]. Additional absorption features resolved at 1081.77 cm^{-1}, 864.33 cm^{-1}, and 753.00 cm^{-1} further corroborate the complex aromatic substitution patterns and out-of-plane (C–H) bending modes of the polyphenol network.

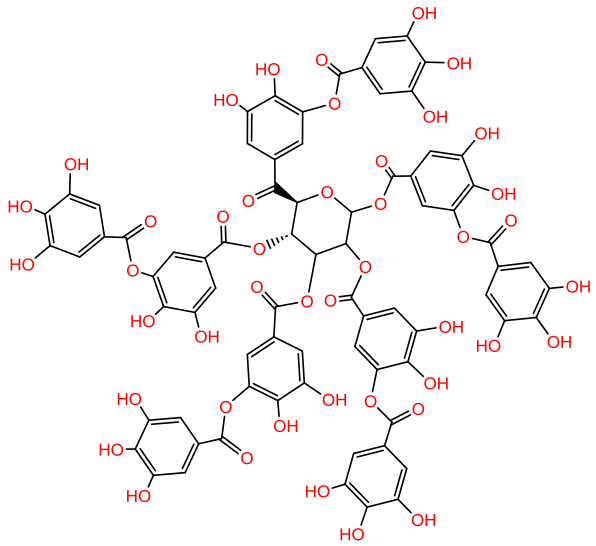

Figure 3. A typical schematic structure of commercial tannic acid used as reference standard

A comparative overlay of the FTIR spectra revealed that the broad ν(O–H) stretching band of reference commercial tannic acid at 3191.22 cm^{-1} shifted to 3246.65 cm^{-1} in the crude ethanolic extract and 3311.53 cm^{-1} in the n-butanol fraction of Quercus robur stem bark (Figures 4 and 5). In contrast, among the three samples, this band was very weak in the crude ethanolic extract, yet mostly pronounced and of the highest intensity in the n-butanol fraction, indicating a potential higher abundance of (O–H) groups. Similarly, prominent υ(C–H) stretching peaks were observed at 2927.62 and 2870.13 cm^{-1} for the n-butanol fraction; whereas a clear band in this region was difficult to resolve in the crude extract. Furthermore, carbonyl υ(C=O) stretching bands were identified at 1706.07 cm^{-1} and 1701.96 cm^{-1} in the crude extract and n-butanol fraction, respectively.

The FT-IR spectra also display key absorption frequencies that closely resemble those of the reference tannic acid. Specifically, the peaks observed at 1609.02 cm^{-1} and 1606.78 cm^{-1} correspond to aromatic υ(C=C) stretching vibrations. This correspondence extends to the band at 1442.83 cm^{-1} υ(C–H) methine bending), the signals at 1330.36 cm^{-1} and 1304.98 cm^{-1} assigned to the symmetric υ(–COO–) stretching), and the ether linkages identified by bands at 1174.86 cm^{-1} and 1010.23 cm^{-1} υ(C–O–C) groups).

It is observed that specific vibrational bands present in the *n*-butanol fraction are absent in the crude extract. This phenomenon is likely due to a combination of concentration effects, the removal of overlapping or masking species, and matrix effects. As bioactive compounds in plant materials exist as complex multicomponent mixtures, their effective separation and characterization often present significant analytical challenges [19, 20]. Furthermore, discrepancies between the n-butanol fraction and the commercial tannic acid spectrum were observed; specifically, certain peaks appearing in the *n*-butanol fraction were absent in the pure tannic acid as reference. This variation is attributed to the presence of co-extracted secondary metabolites within the fraction, which act as impurities relative to the purified commercial standard. Consequently, further purification via column chromatography will be employed to isolate the target constituents.

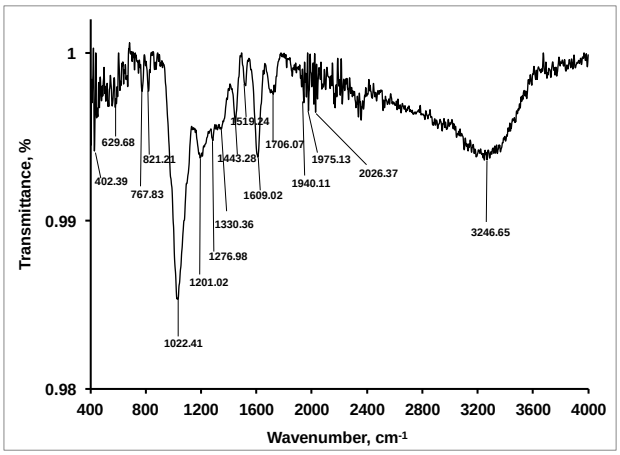

Figure 4. FT-IR of crude ethanolic extract of *Quercus robur*

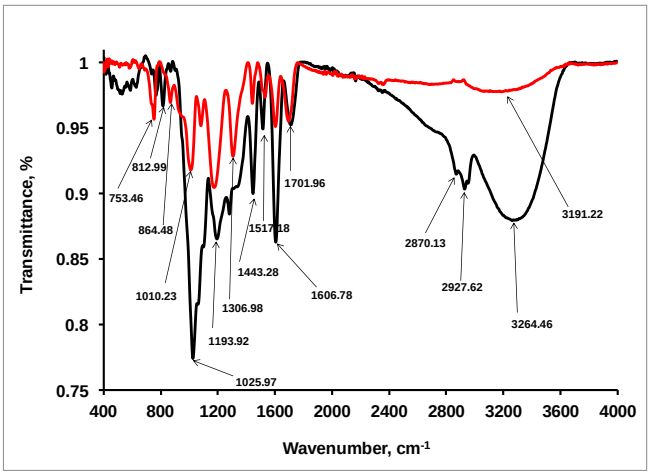

Figure 5. Comparative FT-IR of Commercial Tannic acid and *n*-Butanol fraction

3.3 Quantitative Determination of Tannin Contents by UV-Visible Spectrophotometry

The total tannin content (TTC) of both the crude extract and n-butanol fraction was determined spectrophotometrically and expressed as tannic acid equivalents (TAE) per gram of dry weight. Initially, the TTC of the crude aqueous-ethanol extract of Quercus robur stem bark was calculated as 70.8 mg TAE/g^{-1} of dry weight (7.08 % w/w). After liquid-liquid fractionation of the total crude extract to obtain n-butanol fraction, the resulting fraction was analyzed under previous identical conditions for the crude ethanolic extract. Using the standard calibration curve (A = 0.012C + 0.02) and linearity range (57.3 to 80.8 mg L^{-1}), the measured absorbance (A = 0.87) corresponded to a solution concentration of 70.83 mg L^{-1}. Taking into account the initial sample mass, final volumetric dilution, and dilution factor, the total tannin content (TTC) of the n-butanol fraction was calculated as 225.0 mg TAE g^{-1} dry weight (22.5 % w/w on a dry weight basis). This reflects a successful and approximately threefold enrichment of the active polyphenolic components in the n-butanol fraction compared to the primary crude ethanolic extract. This significant enhancement is fundamentally attributed to selective solvent-solvent partitioning, where polar polyphenolic components (including tannins) are preferentially extracted into the n-butanol fraction while all extraneous, non-active matrix components are separated out.

3.4 Potentiodynamic Polarization Analysis of St3 Steel in 1.0 M HCl

The inhibitory properties of the crude ethanolic extract and the n-butanol fraction of Quercus robur were evaluated using potentiodynamic polarization and compared against commercial tannic acid. Potentiodynamic polarization curves were recorded for both extracts and the reference control in 1.0 M HCl.

Potentiodynamic polarization measurements were conducted to compare the corrosion-inhibition performance of the crude ethanolic extract and the n-butanol fraction of Quercus robur bark against a commercial tannic acid control. As shown in Figures 6-8, the polarization curves enabled comparison of the corrosion-inhibition performance of the investigated samples and assessment of changes in the anodic and cathodic polarization behavior.

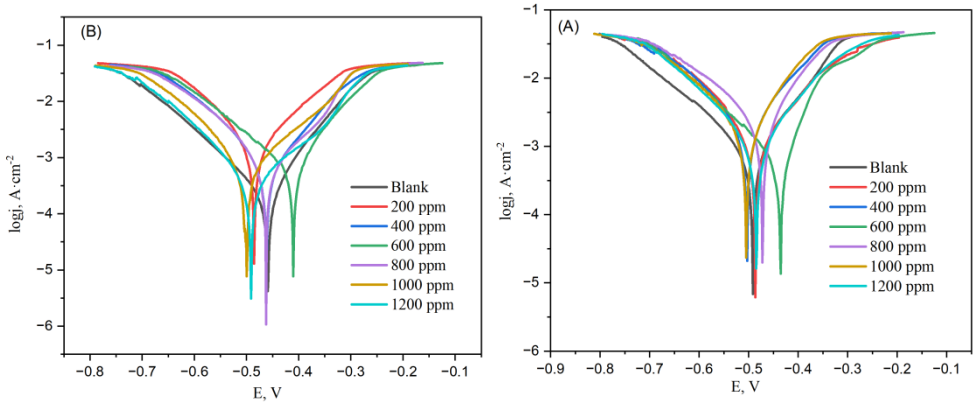

Figure 6. Potentiodynamic polarization curves of mild steel in 1 M HCl solution at different concentrations of the crude ethanolic extract after 0 h (A) and 1 h (B) immersion at 298 K

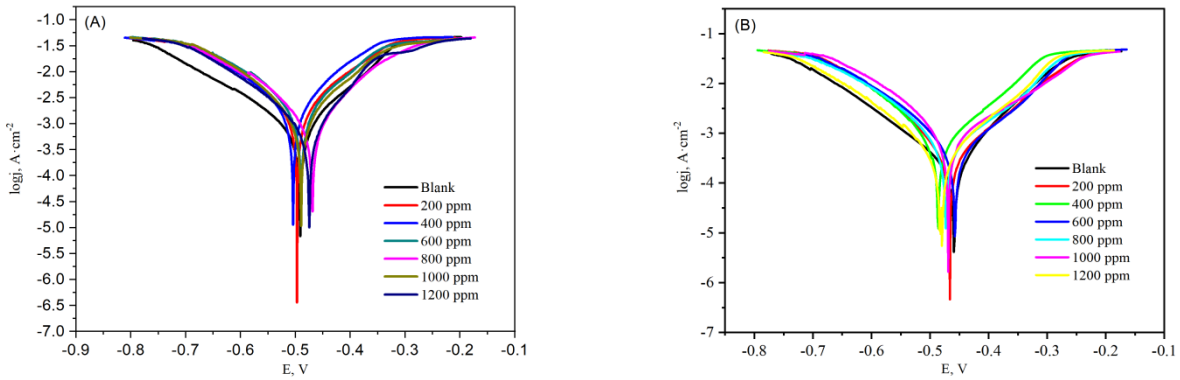

Figure 7. Potentiodynamic polarization curves of mild steel in 1 M HCl solution at different concentrations of the *n*-butanol fraction after 0 h (A) and 1 h (B) immersion at 298 K

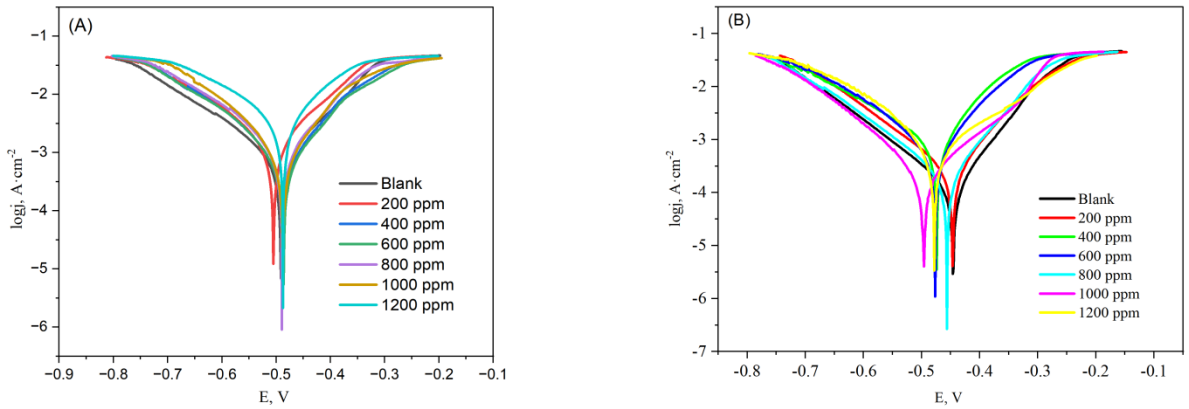

Figure 8. Potentiodynamic polarization curves of mild steel in 1 M HCl solution at different concentrations of commercial tannic acid after 0 h (A) and 1 h (B) immersion at 298 K

A comparative analysis of the potentiodynamic polarization curves revealed that the addition of both the crude ethanolic extract and the *n*-butanol fraction produced changes in both the anodic and cathodic polarization branches, while displacing the corrosion potential (E_{corr}), indicating changes in the electrochemical corrosion behavior. Consequently, the corrosion rate (C_R) decreased while the inhibition efficiency (η) improved across both treatments (Tables 1-6). Although the *n*-butanol fraction elicited a more substantial reduction in corrosion current density than the crude extract, consistent with its higher inhibition efficiency compared with the crude extract, both natural extracts demonstrated a comparatively attenuated inhibitory effect relative to commercial tannic acid, as evidenced by the magnitude of current density reduction and polarization curve displacement.

These observed disparities in inhibitory efficacy are plausibly ascribed to differences in chemical composition and the relative abundance of active constituents contributing to the observed corrosion inhibition behavior. Furthermore, these findings substantiate the capacity of both the crude extract and the *n*-butanol fraction to suppress electrochemical corrosion, underscoring the viability of investigating these botanical extracts as sustainable, eco-friendly corrosion inhibitors.

Table 1

Electrochemical polarization potentiodynamic data for mild steel at different concentrations of crude ethanolic extract, in 1 M HCl, at 298 K, at 0 hour immersion time

C_{inh}, mg L^{-1}	E_{corr}, mV	j_{corr}, μA/cm^2	β_a	β_c	C_R, mm/year	η, %
0	-491.94 ± 2.16	752.52 ± 10.74	148.76 ± 1.80	83.93 ± 2.57	8.74 ± 0.02	
200	-503.78 ± 3.25	850.48 ± 14.23	60.30 ± 1.76	49.24 ± 1.98	9.88 ± 0.01	-
400	-485.52 ± 1.98	695.80 ± 10.92	65.17 ± 1.35	74.10 ± 2.63	8.08 ± 0.02	7.54 ± 0.78
600	-436.68 ± 2.36	673.49 ± 12.67	121.24 ± 1.56	67.77 ± 2.19	7.83 ± 0.03	10.50 ± 0.65
800	-471.46 ± 2.76	619.70 ± 13.02	34.54 ± 1.33	33.85 ± 1.79	7.20 ± 0.03	17.65 ± 0.89
1000	-504.19 ± 1.63	553.87 ± 11.89	32.54 ± 1.89	36.21 ± 2.08	6.62 ± 0.02	26.39 ± 0.90
1200	-484.41 ± 1.85	496.42 ± 10.77	57.46 ± 1.27	37.17 ± 1.65	5.61 ± 0.03	34.03 ± 0.91

Table 2

Electrochemical polarization potentiodynamic data for mild steel at different concentrations of crude ethanolic extract, in 1 M HCl, at 298 K, at 1 hour immersion time

C_{inh}, mg L^{-1}	E_{corr}, mV	j_{corr}, μA/cm^2	β_a	β_c	C_R, mm/year	η, %
0	-458.74 ± 1.86	723.12 ± 12.87	143.75 ± 1.09	135.65 ± 1.87	8.69 ± 0.01	
200	-487.64 ± 2.32	506.98 ± 11.69	34.52 ± 1.67	40.00 ± 2.19	5.89 ± 0.02	29.89 ± 0.74
400	-461.96 ± 3.45	453.57 ± 13.42	63.98 ± 1.84	72.63 ± 2.78	5.27 ± 0.02	37.27 ± 0.86
600	-411.86 ± 1.99	321.88 ± 10.98	46.25 ± 1.49	40.86 ± 2.93	3.74 ± 0.01	55.48 ± 0.91
800	-463.90 ± 2.35	285.95 ± 11.83	42.29 ± 1.78	42.04 ± 1.98	3.32 ± 0.03	60.46 ± 0.87
1000	-502.21 ± 2.78	245.72 ± 11.69	199.88 ± 1.91	27.27 ± 1.84	2.86 ± 0.01	66.02 ± 0.68
1200	-490.21 ± 1.97	203.15 ± 12.86	60.70 ± 1.69	52.44 ± 2.09	2.36 ± 0.03	71.91 ± 0.79

Table 3

Electrochemical polarization potentiodynamic data for mild steel at different concentrations of *n*-BuOH fraction, in 1 M HCl, at 298 K, at 0 hour immersion time

C_{inh}, mg L^{-1}	E_{corr}, mV	j_{corr}, μA/cm^2	β_a	β_c	C_R, mm/year	η, %
0	-491.94 ± 2.16	752.52 ± 10.74	148.76 ± 1.80	83.93 ± 2.57	8.74 ± 0.02	
200	-499.64 ± 1.96	739.66 ± 12.43	50.14 ± 1.43	50.48 ± 1.78	8.59 ± 0.02	1.71 ± 0.76
400	-505.89 ± 2.56	728.30 ± 11.87	54.29 ± 1.56	40.09 ± 1.66	8.46 ± 0.03	3.22 ± 0.84
600	-490.54 ± 2.54	688.75 ± 13.21	44.87 ± 1.67	44.40 ± 2.07	8.00 ± 0.03	8.47 ± 0.59
800	-470.39 ± 1.99	671.38 ± 11.65	80.00 ± 1.75	62.32 ± 1.91	7.80 ± 0.01	10.78 ± 0.92
1000	-489.43 ± 3.14	533.13 ± 12.36	47.01 ± 1.86	41.26 ± 1.77	6.19 ± 0.02	29.15 ± 0.89
1200	-475.58 ± 1.95	479.12 ± 12.86	93.04 ± 1.98	47.15 ± 1.87	5.56 ± 0.02	36.33 ± 0.77

Table 4

Electrochemical polarization potentiodynamic data for mild steel at different concentrations of *n*-BuOH fraction, in 1 M HCl, at 298 K, at 1 hour immersion time

C_{inh}, mg L^{-1}	E_{corr}, mV	j_{corr}, μA/cm^2	β_a	β_c	C_R, mm/year	η, %
0	-458.74 ± 1.86	723.12 ± 12.87	143.75 ± 1.09	135.65 ± 1.87	8.69 ± 0.01	
200	-468.28 ± 1.99	493.82 ± 12.06	142.70 ± 1.86	142.38 ± 1.93	5.73 ± 0.01	31.71 ± 0.74
400	-488.07 ± 2.78	376.70 ± 11.67	88.95 ± 2.31	134.37 ± 1.58	5.53 ± 0.02	47.91 ± 0.86
600	-504.36 ± 1.87	265.04 ± 13.85	83.85 ± 1.73	113.17 ± 1.85	3.08 ± 0.03	63.35 ± 0.91
800	-473.07 ± 3.04	220.12 ± 11.98	37.76 ± 2.34	47.39 ± 1.90	2.56 ± 0.02	69.56 ± 0.78
1000	-470.18 ± 3.46	215.64 ± 12.75	23.64 ± 1.84	35.25 ± 1.88	2.50 ± 0.01	70.17 ± 0.82
1200	-480.58 ± 2.54	148.43 ± 13.09	50.78 ± 1.98	19.52 ± 1.49	1.72 ± 0.02	79.47 ± 0.67

Table 5

Electrochemical polarization potentiodynamic data for mild steel at different concentrations of commercial tannic acid, in 1 M HCl, at 298 K, at 0 hour immersion time

C_{inh}, mg L^{-1}	E_{corr}, mV	j_{corr}, μA/cm^2	β_a	β_c	C_R, mm/year	η, %
0	-491.94 ± 2.16	752.52 ± 10.74	148.76 ± 1.80	83.93 ± 2.57	8.74 ± 0.02	
200	-505.86 ± 2.75	1065.02 ± 15.04	62.50 ± 1.97	50.41 ± 1.98	12.37 ± 0.02	-
400	-488.86 ± 1.97	790.45 ± 12.76	138.38 ± 2.04	106.74 ± 1.85	9.18 ± 0.03	-
600	-487.82 ± 2.67	408.38 ± 11.87	66.78 ± 1.67	65.54 ± 1.76	4.75 ± 0.03	45.73 ± 0.85
800	-489.40 ± 3.09	354.68 ± 13.89	33.46 ± 1.84	33.59 ± 2.12	3.42 ± 0.01	52.87 ± 0.76
1000	-487.86 ± 2.86	211.28 ± 11.67	26.78 ± 1.56	24.46 ± 1.86	2.45 ± 0.02	71.92 ± 0.91
1200	-487.91 ± 1.94	92.87 ± 12.88	6.05 ± 1.95	8.21 ± 1.69	1.07 ± 0.02	87.66 ± 0.87

Table 6

Electrochemical polarization potentiodynamic data for mild steel at different concentrations of commercial tannic acid, in 1 M HCl, at 298 K, at 1 hour immersion time

C_{inh}, mg L^{-1}	E_{corr}, mV	j_{corr}, μA/cm^2	β_a	β_c	C_R, mm/year	η, %
0	-458.74 ± 1.86	723.12 ± 12.87	143.75±1.09	135.65 ± 1.87	8.69 ± 0.01	
200	-459.72 ± 2.05	224.90 ± 13.76	74.52±1.37	60.22 ± 1.65	2.61 ± 0.02	68.89 ± 0.62
400	-425.64 ± 1.98	196.67 ± 12.87	99.23±1.62	70.65 ± 1.50	2.28 ± 0.03	72.80±0.76
600	-451.00 ± 2.67	104.94 ± 14.64	122.75 ± 1.39	83.59 ± 1.47	2.15 ± 0.03	85.45 ± 0.81
800	-441.35 ± 1.83	14.76 ± 1.60	13.69±1.73	13.19 ± 2.61	0.17±0.03	97.95 ± 0.56
1000	-473.16 ± 3.17	12.75 ± 0.99	7.19±2.17	5.78 ± 2.58	0.15±0.02	98.23 ± 0.77
1200	-447.11 ± 2.74	28.72 ± 4.07	4.10±1.89	5.37 ± 1.94	0.33 ± 0.01	96.03 ± 0.85

The influence of exposure duration on corrosion-inhibition efficiency was systematically evaluated. Commercial tannic acid, evaluated as a reference standard, achieved a maximum inhibition efficiency of

98.2 % at 1000 mg L^{-1} after 1 hour of immersion. A further increase in concentration to 1200 mg L^{-1} resulted in a slight decrease in inhibition efficiency to 96.2 %, indicating a non-monotonic concentration response at the highest investigated concentration. The origin of this decrease cannot be determined from the present potentiodynamic polarization data alone.

The *n*-butanol fraction showed higher inhibition efficiency than the crude ethanolic extract under the investigated conditions. At 800 mg L^{-1}, its inhibition efficiency reached 69.5 %, increasing to 79.5 % at 1200 mg L^{-1}. This trend is consistent with the higher tannic-acid-equivalent content measured for the *n*-butanol fraction, although the specific chemical constituents responsible for the improved inhibition performance were not identified in the present study.

Both the crude ethanolic extract and the *n*-butanol fraction showed lower inhibition efficiencies than commercial tannic acid. This difference may reflect differences in chemical composition and the relative abundance of electrochemically active constituents in the investigated samples. However, because the crude extract and the *n*-butanol fraction are complex multicomponent mixtures, the contribution of individual constituents to the observed inhibition behavior cannot be resolved from the present data.

Changes were observed in both the anodic and cathodic branches of the polarization curves for the investigated samples. Together with the relatively small shifts in E_{corr}, not exceeding 85 mV in either direction, these observations support classification of the tannin-containing samples as mixed-type inhibitors. The polarization data therefore indicate an influence on both anodic and cathodic corrosion processes. However, the present measurements do not directly establish the formation of a specific protective adsorption layer, blocking of individual active sites, or changes in elementary electrochemical steps. Such mechanisms may be consistent with previous reports on tannin-containing corrosion inhibitors but would require complementary surface-sensitive or impedance measurements for direct confirmation.

3.5 Adsorption Isotherms

To investigate the concentration-dependent adsorption behavior of the inhibitor species on the mild-steel surface, the apparent surface-coverage data were fitted using the Langmuir, Freundlich, and Temkin adsorption isotherm models [21]. These models were compared using their respective fitting parameters and coefficients of determination (R^2) [22].

The apparent surface coverage (θ) was estimated from the inhibition efficiency obtained after 1 h of immersion in 1 M HCl according to:

$$\theta = \frac{\eta}{100} \tag{3}$$

where η is the inhibition efficiency expressed as a percentage. Because the surface coverage was derived from electrochemical inhibition efficiency rather than measured directly, the calculated θ values are referred to here as apparent surface coverage [21].

The calculated apparent surface coverage generally increased with increasing inhibitor concentration. For commercial tannic acid, θ reached 0.982 at 1000 mg L^{-1}, whereas the corresponding values for the crude ethanolic extract and the n-butanol fraction at 1200 mg L^{-1} were 0.719 and 0.795, respectively.

Table 7

Inhibition efficiency-derived apparent surface coverage values for the crude ethanolic extract, n-BuOH fraction, and commercial tannic acid on mild steel in 1 M HCl at 298 K after 1 h of immersion

C_{inh}, mg L^{-1}	Crude ethanolic extract, θ	*n*-BuOH fraction, θ	Commercial Tannic acid, θ
200	0.299 ± 0.008	0.317 ± 0.007	0.689 ± 0.005
400	0.373 ± 0.004	0.479 ± 0.006	0.728 ± 0.008
600	0.555 ± 0.006	0.633 ± 0.004	0.855 ± 0.004
800	0.605 ± 0.007	0.695 ± 0.003	0.979 ± 0.003
1000	0.660 ± 0.004	0.702 ± 0.008	0.982 ± 0.006
1200	0.719 ± 0.005	0.795 ± 0.006	0.962 ± 0.007

The adsorption data were fitted to the linearized forms of the Langmuir, Freundlich, and Temkin isotherms. The Langmuir model was expressed as [22]:

$$\frac{C}{\theta} = \frac{1}{K_{ads}} + C \tag{4}$$

where C is the inhibitor mass concentration expressed in mg L^{-1}, θ is the apparent surface coverage, and K_{ads} is the apparent mass-based adsorption constant.

The Freundlich isotherm was expressed in its linearized form as:

$$\log\theta = \log K_F + \frac{1}{n}\log C \tag{5}$$

where K_F is the Freundlich adsorption constant and n is the Freundlich heterogeneity parameter.

The Temkin isotherm was expressed in its linearized form as:

$$\theta = B_T \ln A_T + B_T \ln C \tag{6}$$

where A_T is the Temkin equilibrium binding constant and B_T is the Temkin constant related to the variation of adsorption energy.

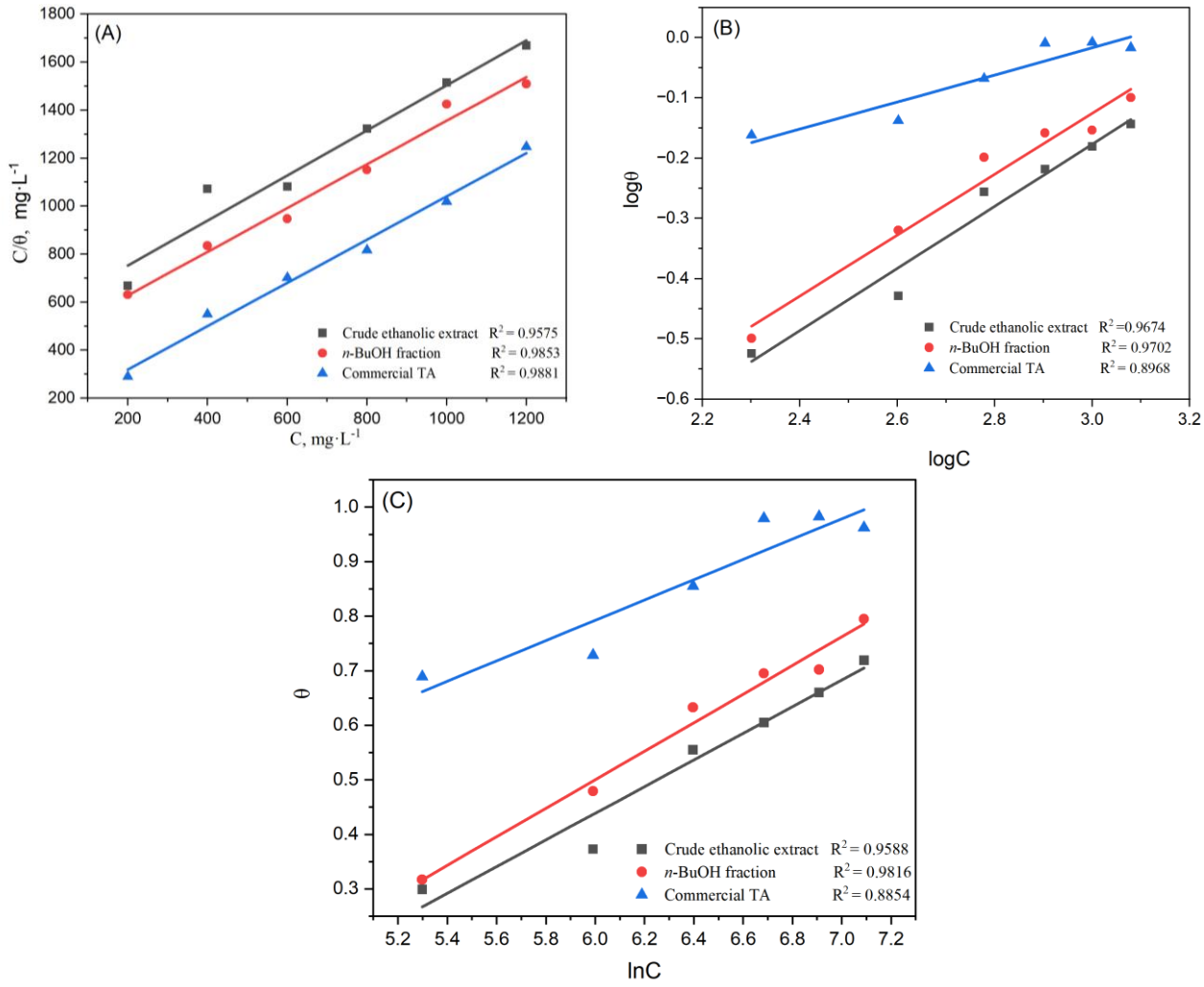

Figure 9. Linearized adsorption-isotherm plots for the crude ethanolic extract, *n*-BuOH fraction, and commercial tannic acid on mild steel in 1 M HCl at 298 K after 1 h of immersion: (A) Langmuir, (B) Freundlich, and (C) Temkin models.

Table 8

Adsorption-isotherm parameters and coefficients of determination (R^2) for the investigated tannin-containing inhibitors on mild steel in 1 M HCl at 298 K

Model	Parameter	Crude extract	n-BuOH fraction	Commercial TA
Langmuir	K_{ads}^{app}, L mg^{-1}	1.77×10^{-3}	2.24×10^{-3}	7.14×10^{-3}
	(R^2)	0.9575	0.9853	0.9881
Freundlich	(K_F)	0.0939	0.0851	0.4736
	(n)	1.78	1.66	2.33
	(R^2)	0.9674	0.9702	0.8968
Temkin	(A_T)	0.0353	0.0389	0.0462
	(B_T)	0.51578	0.50529	0.22492
	(R^2)	0.9588	0.9816	0.8854

Note. All adsorption-isotherm parameters were derived using inhibitor concentrations expressed on a mass-concentration basis (mg L^{-1}). Accordingly, the Langmuir constants are reported as apparent mass-based adsorption constants (K_{ads}^{app}, L mg^{-1}). The Freundlich and Temkin parameters are likewise reported on the same mass-concentration basis and are used primarily for comparison of model fitting.

Comparison of the goodness-of-fit parameters showed that no single adsorption isotherm model provided the best fit for all three investigated samples. For the crude ethanolic extract, the Freundlich model showed the highest coefficient of determination (R^2=0.9674), compared with the Temkin (R^2=0.9588) and Langmuir (R^2=0.9575) models. However, the relatively small differences among the R^2 values indicate that the adsorption behavior of the crude extract cannot be unambiguously assigned to a single model. The slightly better agreement with the Freundlich model may reflect the heterogeneous nature of adsorption from this multicomponent mixture.

For the *n*-BuOH fraction, the Langmuir model provided the highest coefficient of determination (R^2=0.9853), followed closely by the Temkin (R^2=0.9816) and Freundlich (R^2=0.9702) models. For commercial tannic acid, the Langmuir model clearly provided the best fit (R^2=0.9881), whereas considerably lower values were obtained for the Freundlich (R^2=0.8968) and Temkin (R^2=0.8854) models.

Overall, these results indicate that the adsorption behavior depends on the composition of the inhibitor system. Nevertheless, because the surface coverage values were derived from electrochemical inhibition efficiencies rather than measured directly, the adsorption-isotherm fits should be regarded as empirical descriptions of the concentration-dependent inhibition behavior rather than definitive evidence of a particular molecular adsorption mechanism.

The Langmuir adsorption constants presented in Table 8 were derived using inhibitor concentrations expressed on a mass-concentration basis (mg L^{-1}). Accordingly, the obtained constants are reported as apparent mass-based Langmuir adsorption constants (K_{ads}^{app}). The K_{ads}^{app} values were 1.77×10^{-3}, 2.24×10^{-3}, and 7.14×10^{-3} L mg^{-1} for the crude ethanolic extract, the *n*-BuOH fraction, and commercial tannic acid, respectively.

The crude ethanolic extract and the *n*-BuOH fraction are chemically complex mixtures for which a unique molar mass cannot be defined. Therefore, their experimentally applied mass concentrations were not converted to molar concentrations, and molar adsorption equilibrium constants were not calculated for these samples. Consequently, standard Gibbs free energies of adsorption (ΔG_{ads}^{0}) were not calculated for the crude ethanolic extract or the *n*-BuOH fraction. The corresponding Kadsapp values should instead be interpreted as model-dependent, mass-based parameters describing their concentration-dependent adsorption behavior under the investigated conditions.

On the same mass-concentration basis, the *n*-BuOH fraction exhibited a somewhat higher apparent Langmuir adsorption constant than the crude ethanolic extract (2.24×10^{-3} versus 1.77×10^{-3} L mg^{-1}). This observation is consistent with the generally higher inhibition efficiency of the *n*-BuOH fraction. However, the comparison should be interpreted cautiously because both materials are multicomponent mixtures and the Langmuir model was not the best-fitting model for the crude ethanolic extract. Therefore, these mass-based apparent constants should not be interpreted as directly comparable thermodynamic adsorption affinities.

For commercial tannic acid, which was used as the reference material, the mass concentration was additionally converted to molar concentration using the molecular weight of 1701.20 g mol^{-1} specified by the

manufacturer (Sigma-Aldrich). On this basis, the mass-based Langmuir adsorption constant (K_{ads}^{app} =7.14×10^{-3} L mg^{-1}) corresponds to a molar adsorption constant of 1.22×10^{4} L mol^{-1}.

The standard Gibbs free energy of adsorption for commercial tannic acid was calculated according to:

$$\Delta G_{ads}^{0} = -RTln\left(55.5K_{ads}\right) \quad (7)$$

where R is the universal gas constant, T is the absolute temperature (298 K), and 55.5 mol L^{-1} represents the molar concentration of water. The calculated ΔGads◦ value was approximately -33.3 kJ mol^{-1}, indicating that adsorption of commercial tannic acid on the mild-steel surface is thermodynamically favorable under the investigated conditions.

In contrast, ΔG_{ads}^{0} was not calculated for the crude ethanolic extract or the *n*-BuOH fraction because these samples are complex mixtures without uniquely defined molar masses; therefore, conversion of their experimentally applied mass concentrations to a physically meaningful molar concentration would require an arbitrary molecular-weight assumption.

4 Conclusions

This study establishes a streamlined extraction and solvent partitioning protocol for *Quercus robur* bark, yielding a crude ethanolic extract and a polyphenolic-(tannin) enriched *n*-butanol fraction. Rather than pursuing the isolation of individual pure constituents, this is a preliminary approach coupled fractional separation with Fourier-transform infrared (FT-IR) spectroscopic profiling to gain vital insights into the functional chemical features driving the corrosion-inhibition performance.

Potentiodynamic polarization measurements demonstrated that the *n*-butanol fraction exhibited higher corrosion-inhibition efficiency than the crude ethanolic extract under the investigated conditions. After 1 h of immersion, the maximum inhibition efficiency of the *n*-butanol fraction reached 79.5 % at 1200 mg L^{-1}, compared with 71.9 % for the crude extract at the same concentration. Commercial tannic acid showed the highest inhibition performance, reaching 98.2 % at 1000 mg·L^{-1}.

Changes in both the anodic and cathodic polarization branches support the classification of the investigated tannin-containing samples as mixed-type inhibitors under the experimental conditions.

Adsorption-isotherm analysis showed model-dependent behavior. The Freundlich model provided the highest R^2 for the crude ethanolic extract, whereas the Langmuir model provided the highest R^2 for the *n*-butanol fraction and commercial tannic acid. Because the apparent surface coverage was derived from electrochemical inhibition efficiency rather than measured directly, these fits should be regarded as empirical descriptions of the concentration-dependent inhibition behavior rather than direct evidence of a specific molecular adsorption mechanism. For chemically defined commercial tannic acid, the calculated ΔG_{ads}^{0} of approximately –33.3 kJ·mol^{-1} indicated thermodynamically favorable adsorption under the investigated conditions.

Overall, solvent fractionation resulted in an *n*-butanol fraction with higher tannic-acid-equivalent content and improved corrosion-inhibition performance compared with the crude ethanolic extract. However, identification of the individual active constituents and direct elucidation of the surface-inhibition mechanism require further phytochemical characterization and complementary surface-sensitive and electrochemical studies.

Funding

This research has been funded by the Ministry of Science and Higher Education of the Republic of Kazakhstan, Grant No. AP 26102663.

*Author Information**

*The authors' names are presented in the following order: First Name, Middle Name and Last Name

Bibisara Dzhalmukhamedovna Burkitbayeva — Doctor of Chemical Sciences, Professor, Head of Laboratory, Chief Research Scientist, Center of Physical-Chemical Methods of Analysis, Al-Farabi Kazakh National University, 050040, Almaty, Kazakhstan; e-mail: bibisaraburkit@gmail.com; https://orcid.org/0000-0002-9113-4471

Adewale Olufunsho Adeloye — Associate Professor, Al-Farabi Kazakh National University, 050040, Almaty, Kazakhstan; e-mail: adeloye.adewale@kaznu.edu.kz; https://orcid.org/0000-0003-1736-5738

Alfira Farukhovna Miftakhova — Candidate of Chemical Sciences, Senior Lecturer, Al-Farabi Kazakh National University, 050040, Almaty, Kazakhstan; e-mail: alfira.miftakhova1@gmail.com; https://orcid.org/0000-0001-5518-7384

Raigul Zhumakhanovna Jumanova — PhD, Lecturer, Al-Farabi Kazakh National University, 050040, Almaty, Kazakhstan; e-mail: raigul0907@gmail.com; https://orcid.org/0009-0007-7320-3676

Gulmira Sembaykyzy Beisenova (*corresponding author*) — PhD, Senior Lecturer, Al-Farabi Kazakh National University, 050040, Almaty, Kazakhstan; e-mail: beisenova.gumi@gmail.com; https://orcid.org/0000-0002-6751-9451

Akmaral Mukhambetovna Argimbayeva — Candidate of Chemical Sciences, Associate Professor, Head of the Department of Analytical, Colloid Chemistry and Technology of Rare Elements, Al-Farabi Kazakh National University, 050040, Almaty, Kazakhstan; e-mail: akmaral.argimbayeva@gmail.com; https://orcid.org/0000-0002-2467-8241

Gulzhan Seit — 2nd-year Doctoral Student, Al-Farabi Kazakh National University, 050040, Almaty, Kazakhstan; e-mail: gulzhan.seit2024@gmail.com; https://orcid.org/0009-0004-0373-3872

Yeldana Galymzhankyzy Bakhytzhan — PhD, Senior Lecturer, Al-Farabi Kazakh National University, 050040, Almaty, Kazakhstan; e-mail: bakhytzhan.yeldana@gmail.com; https://orcid.org/0000-0002-3217-5927

Aruzhan Bekezhankyzy Smail — 2nd-year Master's Student, Al-Farabi Kazakh National University, 050040, Almaty, Kazakhstan; e-mail: arusmail0807@mail.ru; https://orcid.org/0009-0009-4294-1611

Author Contributions

The manuscript was written through contributions of all authors. All authors have given approval to the final version of the manuscript. CRediT: **Bibisara Dzhalmukhamedovna Burkitbayeva** conceptualization, data curation, investigation, methodology, validation, visualization, writing-review & editing; **Adewale Olufunsho Adeloye** formal analysis, methodology, writing-original draft, writing-review & editing; **Alfira Farukhovna Miftakhova** writing-original draft, investigation, data curation, visualization; **Raigul Zhumakhanovna Jumanova** writing-original draft, investigation, data curation, formal analysis, writing-review & editing; **Gulmira Sembaykyzy Beisenova** supervision, project administration, funding acquisition, resources, writing–review & editing; **Akmaral Mukhambetovna Argimbayeva** investigation, validation, formal analysis; **Gulzhan Seit** investigation, data curation, formal analysis; **Yeldana Galymzhankyzy Bakhytzhan** methodology, resources, validation, visualization; **Aruzhan Bekezhankyzy Smail** investigation, visualization, formal analysis.

References

1 Rahim, A., & Kassim, J. (2008). Recent Development of Vegetal Tannins in Corrosion Protection of Iron and Steel. *Recent Patents on Materials Sciencee, 1(3),* 223-231 https://doi.org/10.2174/1874464810801030223

2 Agi, A., Junin, R., Rasol, M., et al. (2018) Treated *Rhizophora mucronata* tannin as a corrosion inhibitor in chloride solution. *PLoS One, 13(8),* e0200595 https://doi.org/10.1371/journal.pone.0200595

3 Scutareanu, P., & Lingeman, R. (1994). Natural Content of Phenols and Tannin in Quercus Robur Leaves Related to Development of Euproctis Chrysorrhoea Caterpillars. *Acta Horticulturae,* (381), 738–741. https://doi.org/10.17660/actahortic.1994.381.106

4 Ferreira, D., Gross, G.G., Hagerman, A.E., Kolodziej, H., & Yoshida, T. (2008) Tannins and related polyphenols: Perspectives on their chemistry, biology, ecological effects, and human health protection. *Phytochem. 69*, 3006-3008 https://doi.10.1016/j.phytochem.2008.10.018.

5 Gonzalez-Iglesias, D., Rubio, L., Martinez-Vazquez, F., Castillo, A., Celeiro, M., Garcia-Jares, C., Lores, M. (2025). Phytochemical and antioxidant comparison of Quercus ilex and Quercus robur acorn extracts obtained by matrix solid-phase dispersion. *RSC Advances, 15(16),* 12538–12546. https://doi.org/10.1039/d4ra08675a.

6 Qi, C., Li, Z., Bi, H., & Dam-Johansen, K. (2024) Towards sustainable steel corrosion protection: expanding the applicability of natural hydrolyzable tannin in epoxy coatings via metal complexation. *Electrochimica Acta*, *497*, 144546. https://doi.org/10.1016/j.electacta.2024.144546

7 Oki, M., Charles, E., Alaka, C., & Oki, T.K. (2011) Corrosion inhibition of mild steel in hydrochloric acid by tannins from *Rhizophora racemosa*. *Mat. Sci. App*., 02, 592–595 https://doi.10.4236/msa.2011.26079

8 Proença, C.S., Serrano, B., Correia, J., & Araújo, M.E.M. (2022) Evaluation of tannins as potential green corrosion inhibitors of aluminium alloy used in aeronautical industry. *Metals*, *12*, 508. https://doi.org/10.3390/met12030508

9 Qi, C., Li, Z., Bi, H., & Dam-Johansen, K (2024) Towards sustainable steel corrosion protection: Expanding the applicability of natural hydrolyzable tannin in epoxy coatings via metal complexation. *Electrochimica Acta*, *497*, Article 144546. https://doi.org/10.1016/j.electacta.2024.144546

10 Kaco, H., Talib, N.A.A., Zakaria, S., Jaafar, S.N.S., Othman, N.K., Chia, C.H., & Gan, S. (2018) Enhanced corrosion inhibition using purified tannin in HCl medium, *Malaysian J. Anal. Sci*., 22, 931 — 942 https://mjas.analis.com.my/wp-content/uploads/2019/06/22_6_2.html

11 Vorobyova V., Sikorsky O., Skiba M., Vasyliev, G. (2023) Quebracho tannin as corrosion inhibitor in neutral media and novel rust conversion agent for enhanced corrosion protection. *S. Afr. J. Chem. Eng.*, *44*, 68-80 https://doi.org/10.1016/j.sajce.2023.01.003.

12 Dargahi M., Olsson A.L.J., Tufenkji N., Gaudreault R. (2015) Green technology: tannin-based corrosion inhibitor for protection of mild steel. *Corr. Sci.*, *71*, 1321-1329. https://doi.org/10.5006/1777

13 Azmir, J., Zaidul, I. S. M., Rahman, M. M., Sharif, K. M., Mohamed, A., Sahena, F., Jahurul, M. H. A., Ghafoor, K., Norulaini, N. A. N., & Omar, A. K. M. (2013) Techniques for extraction of bioactive compounds from plant materials: A review. *J. Food Eng.*, *117*, 426-436 https://doi.org/10.1016/j.jfoodeng.2013.01.014

14 Awe, E.O., Adeloye, A., Idowu, T., Olajide, O.A., & Makinde J. (2008). Antinociceptive effect of *Russelia equisetiformis* leave extracts: Identification of its active constituents, *Phytomedicine*, *15*, 301–305. https://doi.org/10.1016/j.phymed.2007.03.012

15 Litvinenko, Y. A., Sassykova, L. R., Sassykova, A. R., Konysbayev, A. T., Aitbayeva, R. R., Abildin, T. S., Kanapiyeva, F. M., Zhakirova, N. K., Zhussupova, A. K., Sendilvelan, S., Bhaskar, K., Gomathi, K., & Hua, R. (2026). Elemental composition, heavy metal accumulation and biologically active substances in wild plants of Kazakhstan. *Sci*, *8*(6), Article 123. https://doi.org/10.3390/sci8060123

16 Dai J., Mumper R.J. (2010) Plant phenolics: extraction, analysis and their antioxidant and anticancer properties. *Molecules*, *15*, 7313-7352. https://doi.org/10.3390/molecules15107313

17 Sylla, T., Pouységu, L., Dacosta, G., Deffieux, D., Monti, J. P., & Quideau, S. (2015) Gallotannins and tannic acid: first chemical syntheses and *in-vitro* inhibitory activity on Alzheimer's amyloid β-peptide aggregation. *Angew. Chem., Int. Ed.*, *54*, 8217-8221 https://doi.org/10.1002/anie.201411606

18 Khanbabaee, K., & van Ree, T (2001) Tannins: Classification and definition. Natural Product Reports, 18(6), 641–649. https://doi.org/10.1039/b101061l

19 Chua, L.S., Lau, C.H., Chew, C.Y., Dawood, D.A.S. (2019) Solvent fractionation and acetone precipitation for crude saponins from *Eurycoma longifolia* extract. *Molecules, 24*, 1416. https://doi.org/10.3390/molecules24071416

20 Vargas-Ramella, M., Ely, J., Favaro-Trindade, C.S., Alves dos Santos, B., Campagnol, P.C.B., Lorenzo, J.M. (2026) Analytical characterization and quantification of plant-derived antioxidants focusing on methods, limitations, and data comparability. *Food Anal. Met*., *19*, 162. https://doi.org/10.1007/s12161-026-03075-y

21 Abeng, F.E., Oji, N.N., Osuwa, K.A. et al. (2026) Thermodynamic study and adsorption characteristics of mild steel corrosion inhibition in 0.1 M solution by orange peels (*Citrus sinensis*). *Discov. Chem*., *3*, 81. https://doi.org/10.1007/s44371-026-00546-3

22 Akinbulumo, O. A., Odejobi, O. J., & Odekanle, E. L. (2020). Thermodynamics and adsorption study of the corrosion inhibition of mild steel by Euphorbia heterophylla L. extract in 1.5 M HCl. Results in Materials, 5, 100074. https://doi.org/10.1016/j.rinma.2020.100074